3D Modeling of Highway Guardrails for Sight Distance Assessment

3D modelling of highway guardrails for sight distance assessment

Alessandra Lioi, MSc

PhD candidate

Department of Environment, Land and Infrastructure Engineering, Politecnico di Torino

ORCID: 0000-0003-0812-4094

César De Santos-Berbel, PhD

Assistant Professor

Departamento de Estructuras y Física de Edificación, Universidad Politécnica de Madrid

ORCID: 0000-0001-9686-8872

Marco Bassani, PhD

Associate Professor

Department of Environment, Land and Infrastructure Engineering, Politecnico di Torino

ORCID: 0000-0003-2560-1497

Maria Castro, PhD

Associate Professor

Departamento de Ingeniería del Transporte, Territorio y Urbanismo, Universidad Politécnica de Madrid

ORCID: 0000-0001-8941-5795

Manuscript accepted in *Journal of transportation Engineering, Part A: Systems*

https://doi.org/10.1061/JTEPBS.0000593

Abstract

Safety barriers limit the severe consequences to occupants of vehicles leaving the roadway from colliding with obstacles, yet they may significantly reduce the available sight distance (*ASD*). A procedure was devised to accurately recreate highway guardrails in three dimensions (3D), fitting the barriers onto the curve roadsides. The effect of these devices on the reduction of the *ASD* was thus evaluated in a set of case studies comprising different curve radii overlapped with different vertical alignments and combined each with two safety barriers in two-lane rural roads. The 3D models of highway curves with the selected guardrails were created in a Geographic Information System. Then, a geoprocessing model was used to compute the *ASD*. The results made possible to quantify the *ASD* reduction produced by the barrier with higher containment level in relation to the highway design parameters, which can assist authorities in developing more comprehensive safety device standards.

Keywords

Guardrails, Highways, Sight distance, Road safety, 3D modelling

Introduction

Road restraint systems are safety devices aimed at protecting drivers and occupants from the consequences of vehicle departure from the carriageway, absorbing the impact energy. Since they contain out-of-control vehicles within the road, the even more serious consequences resulting from an impact against roadside fixed objects or the vehicle rollover are avoided (AASHTO 2018).

Road restraint systems are installed along medians and roadsides, so they limit the driver's ability to see the roadway ahead (Wang et al. 2017). Steinauer and Mayer (1999) observed that on left-hand curves on German motorways crashes are more frequent than on the counterpart right-hand curves due to the sight-distance reduction caused by the median barriers. The limitation of the available sight distance (*ASD*) is often in contrast with the need to guarantee a sufficiently long visible portion of the road ahead where to complete manoeuvres safely. As a result, road designers must satisfy both needs adopting adequate barriers and geometric characteristics preserving a minimum *ASD* from potential conflict points and/or obstacles along the driving path (AASHTO 2018; Ministerio de Fomento 2016; Ministero delle Infrastrutture e dei Trasporti 2001). Sight distance is one of the most important elements not only in the road design but also in the road management to the aim of traffic safety (Castro et al. 2016). Montella (2001) advocated cost-benefit analyses to choose the most appropriate traffic containment device in terms of safety performance. Consequently, given the effects of safety barriers on the *ASD*, it must be included in such analyses (De Santos-Berbel et al. 2018).

The installation and performance requirements of safety barriers in European countries are regulated by European and national standards. As stated by European standards (CEN 2002, CEN 2011a; b, CEN 2012), barriers are classified according to several containment levels, the entity of the deflection of the system and classes of dissipated impact energy. However, each Member State imposes different minimum requirements based on the road characteristics and operating traffic conditions (Ministerio de Fomento 2009, 2014; Ministero delle Infrastrutture e dei Trasporti 2004). Hence, in similar roads operating under similar traffic conditions, barriers of different characteristics

may be installed in the same European country, as well as among countries. In this sense, barriers that oversize the minimum standard requirements may be selected in a precautionary way while significantly altering sight-distance conditions.

The selection of roadside barriers for new construction or safety upgrading involves contemplating the combined effect of highway geometrics with limited sight distance (AASHTO 2011). Sarhan and Hassan (2012) investigated the effect of different concrete barriers on the *ASD* for the stopping maneuver. Nevertheless, studies addressing the impact and consequences in terms of sight distance of installing different guardrails, which have a more complex three-dimensional (3D) shape than concrete barriers, have not been found in the literature. Furthermore, it has been evidenced that small differences in accuracy of 3D road items might produce significant variations in the *ASD* estimation (Bassani et al. 2019; Iglesias et al. 2019). As a consequence, the 3D modelling of road barriers must be carried out with the highest accuracy and precision.

This research aims to devise an advanced procedure to accurately recreate highway sections with guardrails in 3D. Moreover, the procedure was tested for evaluating the effect of two different guardrails on the *ASD* on curves in relation to the highway design parameters.

The paper is divided into five sections. The introduction is followed by a review of the current state of the art. A subsequent section outlines the procedure devised to recreate the guardrails and describes the organization of the case studies. The next section summarizes and discusses the results obtained from the study. Conclusions and brief considerations about future research are presented in the last section.

Related works

The *ASD* is the maximum length of the road stretch ahead measured along the future path that the driver can see in the presence of sight obstructions, i.e. elements of the roadway and/or the roadside (Castro et al. 2016). **Figure 1** illustrates how the *ASD* is measured along the vehicle trajectory as the distance between the farthest point visible (D, detected from the intersection between the line of

92 sight – LOS – and the trajectory itself) and the point of view (A). From the point of view A, straight
93 lines may be built to link target points along the future path (B, C, D, …G); lines AB, AC, …, and AG are
94 sight lines from the driver's eyes. Since the lines AE and AF intersect the sight obstruction (the HI
95 element), the driver cannot see the road stretch from E to F. Hence, he/she can only see the sections
96 from A to D and from G: the *ASD* is, therefore, the arc length from A to D.

97 For safety reasons, the *ASD* must be greater than the distance used to stop the vehicle before
98 hitting an unexpected object along the lane (i.e., the stopping sight distance, *SSD*). Consequently, the
99 *ASD* may be considered in the evaluation of safe speed limits. The comparison between *ASD* and *SSD*
100 allowed assessing the influence of sight distance on road safety. Ibrahim and Sayed (2011)
101 incorporated stochastic risk measures due to insufficient sight distance to a crash prediction model to
102 evaluate the potential impact of horizontal curve design on the collision frequency. By analysing top
103 crash-prone segments, Gargoum and El-Basyouny (2020) showed that the crash frequency is 2 to 3
104 times higher where the required *SSD* is not met.

105

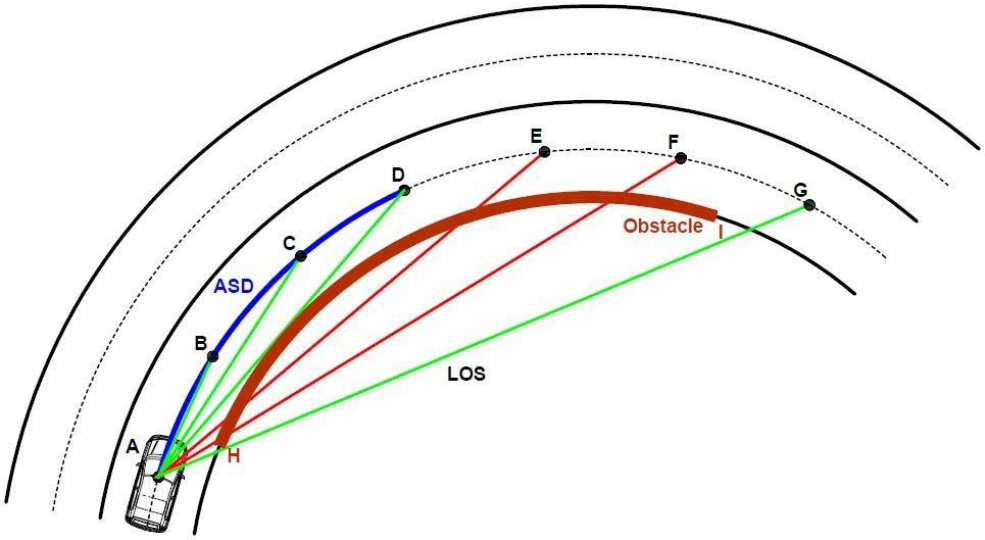

106

107 **Figure 1**. Graphical definition of the available sight distance (*ASD*).

108

109 For the *ASD* analysis, Spanish and Italian highway design standards (Ministerio de Fomento
110 2016; Ministero delle Infrastrutture e dei Trasporti 2001) provide values for the height of the driver's

eye and the height of a possible obstacle, with the driver's head position located at 1.1 m above the pavement surface. Different obstacle heights are assumed in the assessment of *ASD* to check the compliance with the *SSD* requirements: 0.1 m with the Italian standard, and 0.5 m with the Spanish one. For research purposes, the heights of target may be differentiated from the standard values. De Santos-Berbel and Castro (2018) set the driver's eye heights at 1.5 m and 2.0 m to simulate sight-distance scenarios with heavy vehicles in the vicinity of underpasses, producing relevant variations in the *ASD* outputs.

The *ASD* depends on cross-section elements, roadside features, and horizontal and vertical alignment (Ismail and Sayed 2007). On existing roads, reduced sight distance may be caused by inadequate geometric design, changes in the initial roadside conditions due to natural or human actions, or both (De Santos-Berbel et al. 2013).

Although most current design policies contemplate the two-dimensional (2D) approach to evaluate the *ASD*, the literature suggests that a 3D approach is much more reliable to avoid overestimation or underestimation of the *ASD* (Castro et al. 2017). De Santos-Berbel et al. (2018) studied and compared the differences between the output of 2D and 3D ASD analyses produced by concrete barriers on curves on existing highways. The results found significant differences between both procedures. Particularly, the superelevation, the effect of which could be included in the 3D procedure, was found to affect the results. Papadimitriou et al. (2018) highlighted the need to consider the combined effect of 3D alignments alloys and the presence of containment devices.

Many methods and algorithms have been developed and validated for the evaluation of the *ASD*. Several authors have proposed *ASD* estimation procedures based on modelling the surface of the roadway and roadside features to recreate the highway and its environment (Castro et al. 2014; Ismail and Sayed 2007). Liu (2013) developed an analytical method to determine the available sight distance on combinations of vertical and horizontal curves in the presence of roadside barriers. These procedures have shown limitations to represent overhanging features in the road environment. Alternatively, Campoy-Ungría (2015) suggested an *ASD* estimation method based on prismatic line-of-

137 sight buffers launched directly on a high-density LiDAR cloud of points, not requiring any terrain
138 surface. More recently, fully 3D methods have been developed and validated to obtain reliable *ASD*
139 results (Gargoum et al. 2018; Ma et al. 2018; De Santos-Berbel and Castro 2018).

140 Some recent investigations have been focused on the use of mobile laser scanning (MLS) data
141 to obtain point clouds to be used to accurately create 3D models of real driving scenarios along road
142 sections (Alcón Gil et al. 2021; Bassani et al. 2015; Ma et al. 2018; Shalkamy et al. 2020) and
143 intersections (Jung et al. 2018). The difficulties inherent in the use of MLS techniques stem, on the one
144 hand, from the strong dependence of the *ASD* analysis on the accuracy of the objects modelled in the
145 near environment and its modelling procedure to subsequently obtain realistic *ASD* values. Hence, a
146 dense cloud of points is required to enable a proper modelling of the shape of elements that may
147 represent a sight obstruction (Bassani et al. 2019; Iglesias et al. 2019). As a result, a significant amount
148 of data and storage capacity are necessary, with a significant share of data points that are not
149 effectively necessary for the analysis (i.e., inefficient). On the other hand, the use of MLS is, in
150 principle, limited to real scenarios and is not suitable to be used in road design scenarios.
151 Nevertheless, the procedure utilized in this study is capable of incorporating 3D features derived from
152 MLS surveys along with virtual new elements to recreate different scenarios (Alcón Gil et al. 2021; De
153 Santos-Berbel and Castro 2018).

154 To lighten the computational burden and related costs to carry out sight distance calculation,
155 Ma et al. (2019) have introduced the use of a convolutional neural network that enables the
156 estimation of the *ASD* using far fewer points. This algorithm improves the above reported
157 inefficiencies related to the use of large databases from MLS, partially solving the former of the two
158 issues abovementioned.

159 Spatial analysis and environment modelling capabilities of geographic information systems (GIS)
160 have led to the development of *ASD* estimation procedures (Khattak and Shamayleh 2005). Castro et
161 al. (2011) provided a 3D approach based on viewsheds to evaluate *ASD* by using GIS tools. Later on,
162 Castro et al. (2014) provided a more efficient procedure based on algorithms that iterated lines of

sight. Bassani et al. (2016, 2019) evaluated the *ASD* in an urban road scenario where several sight obstruction types are present, intending to highlight and compare the computational efficiency, advantages and drawbacks of GIS and numerical computing codes.

The use of a GIS in highway sight distance studies can help solve part of the difficulties in the use of traditional design software because it can be employed to carry out other geometric and safety analyses. For example, consistency and safety analyses are carried out overlapping with GIS the information coming from crash counts, operating speeds, traffic data, road features, and geometric characteristics of a highway (Castro and De Santos-Berbel 2015; Iglesias et al. 2016). Furthermore, the detection of shortcomings and hidden dips in the 3D alignment can also be carried out in the GIS environment (Castro et al. 2017; Castro and De Santos-Berbel 2015). Road design standards and guides can be used in a GIS to generate realistic 3D road models starting from 2D data including centreline and basic cross-sectional information (Wang et al. 2014). Current GIS applications are robust enough to model road elements and obtaining results comparable to those coming from sight inspections. Finally, GIS is a flexible tool that can also overcome the limitation of MLS based techniques because it can easily include 3D sight obstructions, e.g. objects in the roadside like poles, installations, and safety barriers.

Methodology and materials

This section outlines the procedure to build up the 3D model of the horizontal curves with the selected guardrails for the assessment of the *ASD*. The computer software used to analyse the 3D models is also described.

3D modelling: barrier design

The importance of accurately and precisely modelling the road and its environment in 3D, guardrails included, stems from obtaining reliable results from the analysis. In this sense, these devices must be accurately recreated and adapted to the roadside for any given highway alignment layout. The

assessment of the *ASD* contemplated two different types of guardrails. The first one is a 2-wave N2-type guardrail, which reflects the guardrail typically installed on Spanish two-lane rural highways. The second one is a 3-wave H2-type guardrail, widely used in Italy on the same road type. The process devised to create the 3D barrier models is illustrated in **Figure 2**. All the relevant components of their profile were drawn on computer-aided design software. It is worth noting that the considering elements must be represented with closed lines to facilitate the operations in 3D drawing software used later.

The cross-section drawings displayed in **Figure 3** were imported into SketchUp Pro to create the 3D models. Then, the barrier beam was extruded along a straight guideline perpendicular to the plane containing the beam cross-section. This guideline, represented by the red dotted line in **Figure 4**, serves in turn as the reference line for the installation of the barrier since it is located at the same height as the base of the posts and in the same vertical position as the generating line of the beam closest to the road centreline. Next, the barrier posts were replicated and inserted at the specified fixed distances throughout the barrier (4 m for the N2 type, 2 m for the H2 type), thus obtaining the 3D model of the guardrails displayed in **Figure 4**.

The straight barrier displayed in **Figure 4** serves as a template to create the required barrier models for any highway alignment. SketchUp Pro was selected to take advantage of the CLF Shape Bender extension, which makes it possible to adapt a given shape, not necessarily with a homogeneous cross-section, to a 3D curve given a guideline for the original shape and another guideline for the target shape (Trimble 2013).

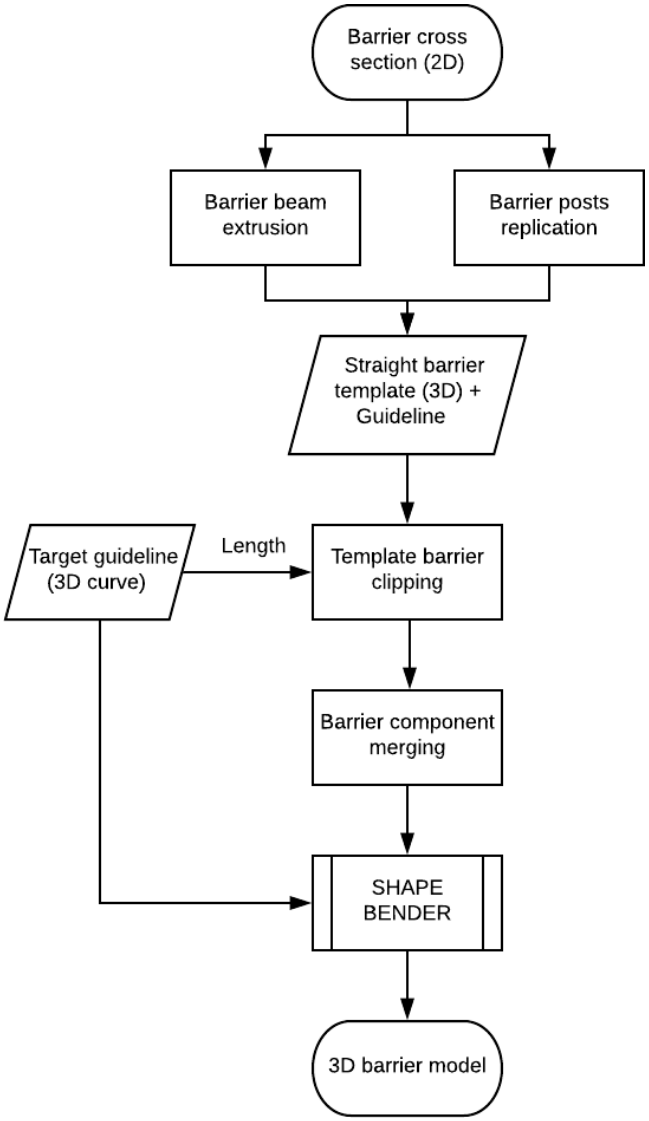

209

210 **Figure 2**. Flowchart of the 3D barrier model creation process.

211

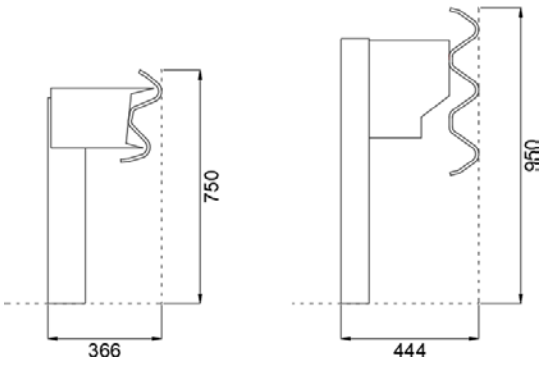

212

213 (a) (b)

214 **Figure 3**. Cross-sections of N2 (a) and H2 (b) metallic barriers (unit of measurement: mm).

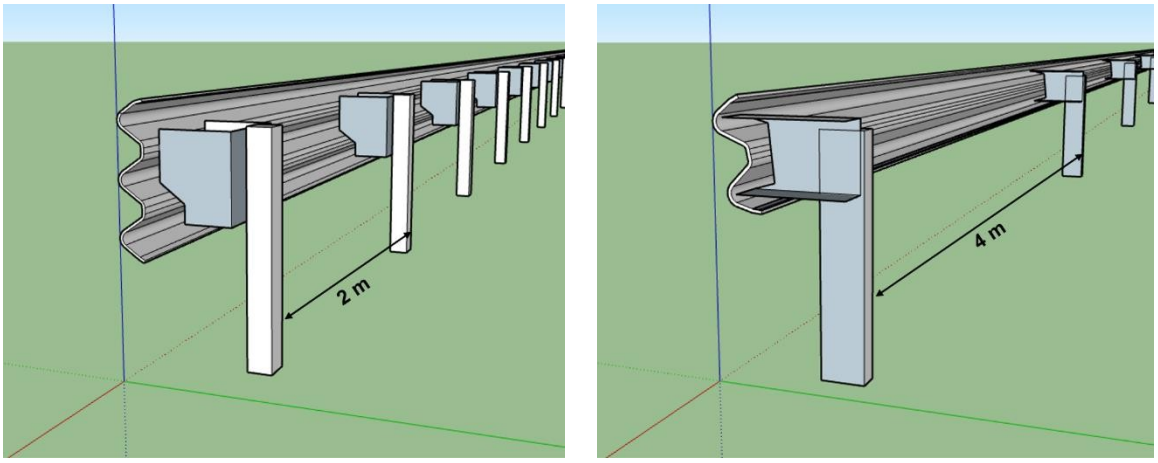

(a) (b)

Figure 4. 3D view of N2 (a) and H2 (b) selected guardrails in SketchUp Pro.

To create a barrier that suits the highway curve in 3D, the 3D curve featuring the roadway inner edge was imported into SketchUp. Next, for producing a barrier without longitudinal distortion, the straight barrier template and its guideline were clipped with length equal to that of the target guideline. Then, all the resulting guardrail components were merged into a single object as required to launch the Shape Bender extension. The 3D guardrail models thus produced were exported as Collaborative Design Activity (COLLADA) format and then imported into a multipatch feature in ArcScene (3D GIS environment), where they were placed in their final position (**Figure 5**). A multipatch feature is a GIS entity whose specific data represent the outer surface of an object, which occupies a volume in the 3D space (ESRI 2008).

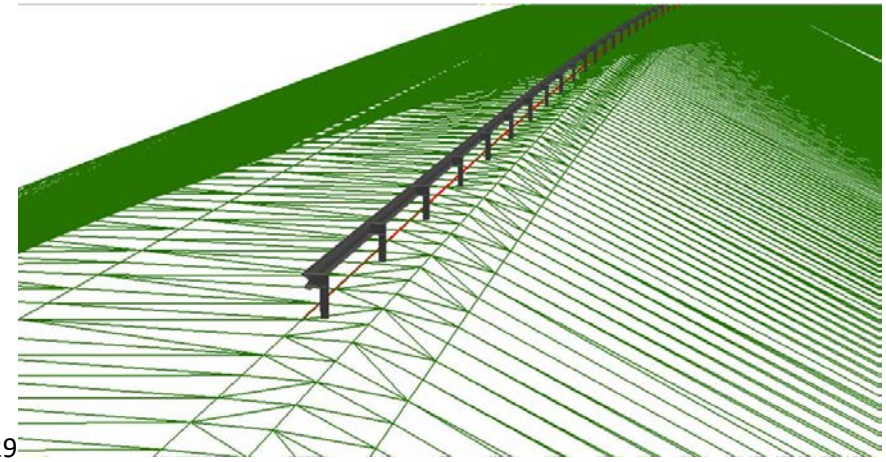

Figure 5. 3D view in ArcScene of N2 guardrail inserted on the TIN model and fitted to the roadside (red line).

Geoprocessing model

Whereas the feature classes representing different types of barriers as visual obstructions that comprise the 3D model were laid out in the 3D environment of ArcScene, the evaluation of the *ASD* was run in ArcMap 10.3. This allowed boosting computation performance while maintaining the 3D nature of the highway model. Numerical results were obtained by using a GIS geoprocessing model developed and validated by the authors (Iglesias et al. 2016; De Santos-Berbel and Castro 2018). This geoprocessing model is based on tools from the 3D Analyst extension of ArcMap and it permits to consider 3D visual obstacles. First, "Construct sight lines", which connects the positions in space of the driver's eye point and the target points (ESRI 2021a). Then a sequential automatic selection of the generated line feature class input the "line of sight" tool along with the elevation model and the multipatch feature class (ESRI 2021b). It evaluated whether each line of sight is obstructed by any of the model features and, if so, returns a new point feature class containing the exact position in space where the lines of sight were obstructed. In addition, the geoprocessing model outputs the sight distance evaluation results from which the *ASD* values are retrieved.

The data required to execute this geoprocessing model includes the theoretical path followed by a vehicle (with stations spaced 5 m apart) and the elevation model which recreates the highway and its roadsides. In general, two types of elevation models are available: digital terrain models (DTM) and digital surface models (DSM). A DTM is a 3D representation of the terrain surface which includes exclusively the elevation of the bare ground, without vegetation, traffic signs, or buildings. On the other hand, DSMs consider the structures on the surface, also detecting overhanging features. Nevertheless, when overhanging features are present by the roadsides (as in the case of safety barriers), the intrinsic features of DSMs do not support two points on its surface having the same horizontal projection and different elevation values (Iglesias et al. 2016; De Santos-Berbel and Castro 2018). To overcome this problem, the highway 3D model was built up combining a DTM and fully-3D modelled landscape features. The former was built up in GIS from a cloud point created using CLIP version 1.29 road design software (TOOL S.A. 2013). The point cloud was created from the most

relevant points of road cross-sections spaced 1 meter apart. Next, a triangular irregular network (TIN) (surface defined by the mesh in **Figure 5**) was built considering the point cloud as the node set. The later comprises the multipatch feature classes modelling the guardrail as a sight obstruction. The procedure allows to include mass standardized constructive elements into the highway 3D model in the GIS environment. Therefore, the method hereby presented provides reliable results thanks to the incorporation of lifelike-modelled 3D objects.

It must be noted that guardrails do not constitute a simple continuous obstacle like vertical surfaces (e.g., walls, rigid concrete barriers), but they might enable the driver to perceive the road ahead through the spaces between posts beneath the barrier beam. In this sense, the capability of the geoprocessing model to return the 3D position of the visual obstruction and identify the visual obstacle that obstructed each line of sight made it possible to accurately assess the *ASD* in the presence of guardrails contemplating its complex 3D shape.

Furthermore, the driver's eye height and the target height are two required input parameters of the geoprocessing model. Their values were taken according to the Spanish highway design standard, as 1.1 and 0.5 m, respectively (Ministerio de Fomento 2016).

The algorithm first launches sightlines connecting the driver's point of view and targets located along the vehicle path ahead, up to a prespecified maximum distance. Next, it checks whether the sightlines are obstructed or not by either the DTM or the inserted multipatch features and retrieves the *ASD* values.

Experimental design

To test the procedure for building up 3D models, a set of highway alignments was created. Nine horizontal curves were designed with different radius, each one connected to spirals at both ends. Two alternative vertical profiles were designed for each curve: a flat-grade profile and a profile with vertical curves overlapped to each horizontal curve according to the alignment coordination principles (Ministerio de Fomento 2016; Ministero delle Infrastrutture e dei Trasporti 2001). The cross-section

284 consists of a 7-m wide travelled way with two lanes (3.50 m each), one per driving direction, and 0.5
285 m-wide shoulders. Since the guardrail was placed in such a way that the horizontal projection of the
286 innermost generatrix of the beam coincides with the outer edge of the shoulder, the lateral offset
287 with respect to the travelled way was 0.5 m. In terms of design speeds, radii, and superelevation of
288 curves, two categories of roads can be distinguished, the so-called *Group 2* and *Group 3* according to
289 the Spanish standard denomination for undivided highways (Ministerio de Fomento 2016).

290 The geometric features of the horizontal curves are provided in Table 1. The length of each
291 curve has been laid out to ensure that the ends of the lines of sight that determine the minimum *ASD*
292 associated to the curve lie within the bounds of the circular arc of the curve on both travelling
293 directions. Table 1 also includes the parameter K_V (equation 1) of the overlapped vertical curve.
294 Negative K_V values correspond to vertical crest curves while positive ones correspond to vertical sag
295 curves. Design speeds in *Group 2* range from 120 to 80 km/h at intervals of 10 km/h. In *Group 3*, design
296 speeds range from 80 to 50 km/h. The design speed values are associated to the minimum radius
297 allowed in a highway segment as indicated in Table 1.

298 $$Kv = 100 \cdot L/\theta \qquad \text{Eq. 1}$$

299

300 where K_V is the vertical curve parameter in m, L is the length of vertical curves in m, and θ is the
301 absolute value of the algebraic difference between the outbound i_2 and inbound i_1 grades in %.

302 To carry out the sight-distance analysis using the geoprocessing model, either guardrail model
303 was set by the inner roadside of each curve. The *ASD* estimation was repeated for both travelling
304 directions.

305

306 **Table 1.** Geometric characteristics of the horizontal curves. The negative value of K_V indicates a crest
307 vertical curve (group 2), a positive value represents a sag vertical curve (group 3).

Group	Section	Horizontal radius (m)	Design speed (km/h)	K_V (m)	Superelevation (%)	SSD (m)
2	Curve 1	700	120	- 38467.98	8	261.49
	Curve 2	550	110	- 30218.00		216.79
	Curve 3	450	100	- 24718.02		178.59
	Curve 4	350	90	- 19218.05		145.48
	Curve 5	250	80	- 13718.10		116.85
3	Curve 6	265	80	+ 14617.94	7	116.85
	Curve 7	190	70	+ 9515.16		91.17
	Curve 8	130	60	+ 6750.37		69.67
	Curve 9	85	50	+ 4198.36		51.73

308

309 As previously stated, the *ASD* along a highway section must meet the distance needed for
310 vehicles to stop (i.e., *ASD* ≥ *SSD*). *SSD* is measured from the driver's position at the time when the
311 obstruction appears and justifies the braking. It includes two contributions: the distance covered by
312 the vehicle from the instant the driver perceives the obstacle to the instant the brake is applied (i.e.,
313 the perception and reaction distance) and the distance needed to stop from the instant the braking
314 maneuver begins (i.e., the braking distance). *SSD* in m is evaluated according to Equation 2:

315 $$SSD = \frac{V \cdot t}{3.6} + \frac{V^2}{254 \cdot (f_l + i)} \quad \text{Eq. 2}$$

316

317 where V is the design speed in km/h, t is the perception and reaction time (2 s, according to the
318 Spanish standard (Ministerio de Fomento 2016), f_l is the longitudinal friction coefficient (as a function
319 of the design speed), and i is the longitudinal grade in %. Table 1 provides *SSD* values for this
320 experiment. In this assessment, the longitudinal grade was neglected due to its small values. **Figure 6**
321 gives the flow chart of the sight distance analysis.

322

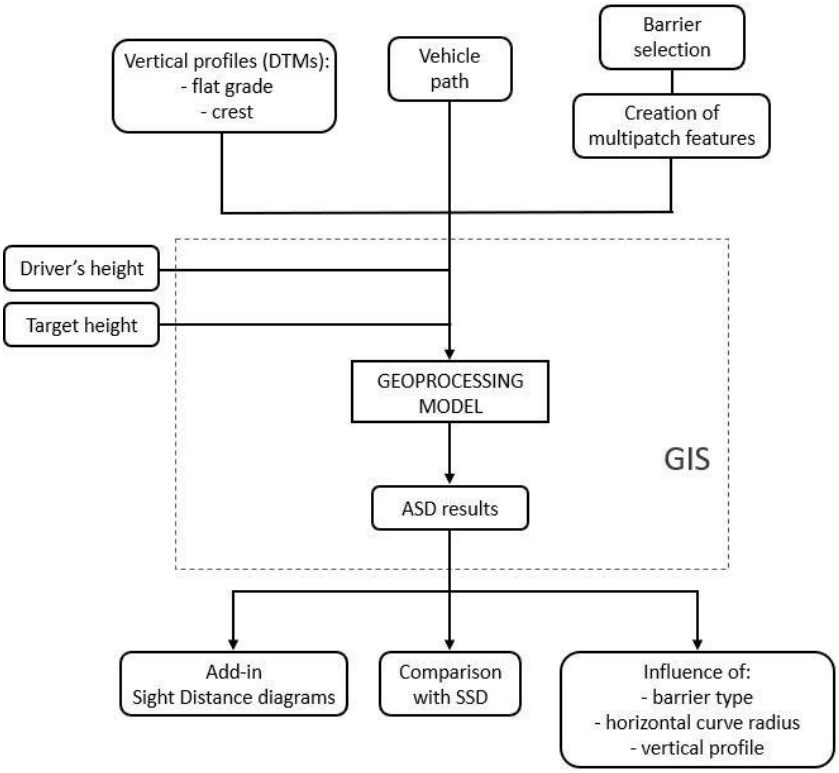

Figure 6. Flow chart of the research study.

By setting the vehicle trajectory and the roadside features, the geoprocessing model elaborated the sight distance diagrams with both profiles. Once the *ASD* values had been extracted, the impact of the barrier type on the *ASD* in function of the horizontal curve radius and the vertical profile was determined.

Results and discussion

The minimum ASD values obtained for each alignment on either travelling direction combined in turn with either guardrail model have been extracted. The aforementioned capability of the geoprocessing model to identify the position and the visual obstacle at which lines of sight are intercepted made it possible to assert that in the case studies the ASD limitation was produced by the barrier beam. Although lines of sight might pass through the gap between the barrier posts, it was checked that these lines did not affect the *ASD* output since the limiting feature was found to be the barrier beam in all cases.

First, horizontal curves overlapped with the flat-grade profile were analyzed with either barrier, discerning between left-hand and right-hand curves (**Figure 7**). Considering that in the absence of visual obstructions the *ASD* would be unlimited, a reduction of the *ASD* is observed in all the curves due to the presence of barriers.

On left-hand curves overlapped with flat-grade profile (**Figure 7**a), the *ASD* is greater than the required *SSD* in all group 3 curves (those with smaller radius) with both barrier types. A greater decrease of the *ASD* with the H2 guardrail due to its higher size is evident. This reduction in *ASD* increases as the radius of the curve increases too. For curves of Group 2, the *ASD* met the required *SSD* in the presence of the 2-wave N2 barrier, except for the curve with R = 700 m (*ASD* = 260 m vs. *SSD* = 216.8 m). The 3-wave H2 barrier does not allow the *ASD* to meet the required *SSD* in curves with a larger radius (e.g. *ASD* = 210 m vs. *SSD* = 261.5 m for R = 700 m).

In right-hand curves (**Figure 7**b), barriers do not guarantee the required *SSD* in almost all the analysed cases, with a greater obstruction given by the 3-wave H2 barrier. The greatest sight distance deficits are observed for the largest radii: with the H2 barrier, the *ASD* values are lower than half of the required *SSD* (e.g. *ASD* = 120 m vs. *SSD* = 261.5 m for R = 700 m). The N2 guardrail provides *ASD* always larger than *SSD* only curves of smaller radius (e.g. group 3, *ASD* = 55 m vs. *SSD* = 51.7 m for R = 85 m).

As expected, results depict that the installation of 2-waves guardrails is less unfavorable than the installation of 3-waves ones in terms of sight distance. All else being equal, the *ASD* is greater in left-hand bends, while in right-hand curves it is more difficult to guarantee it, especially in curves with larger radii.

Since there are two different cases for vertical profiles (flat-grade and with vertical curves), it is possible to compare the effect of the same barrier in different vertical alignments. Figure 8 shows the analyses for N2 barrier, while Figure 9 those for H2 guardrail.

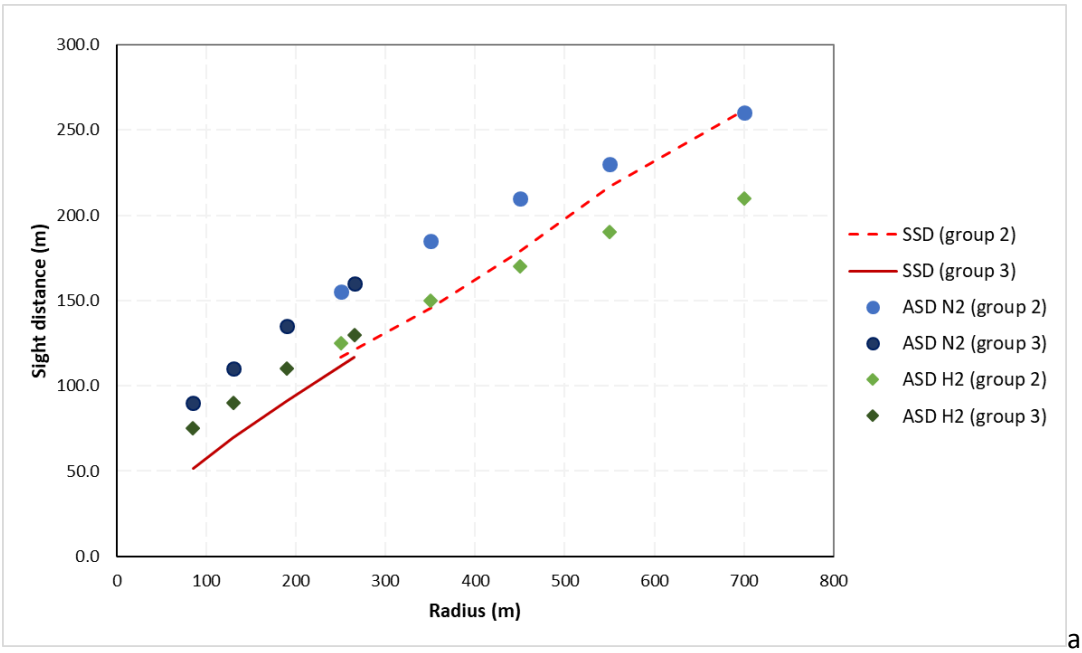

a)

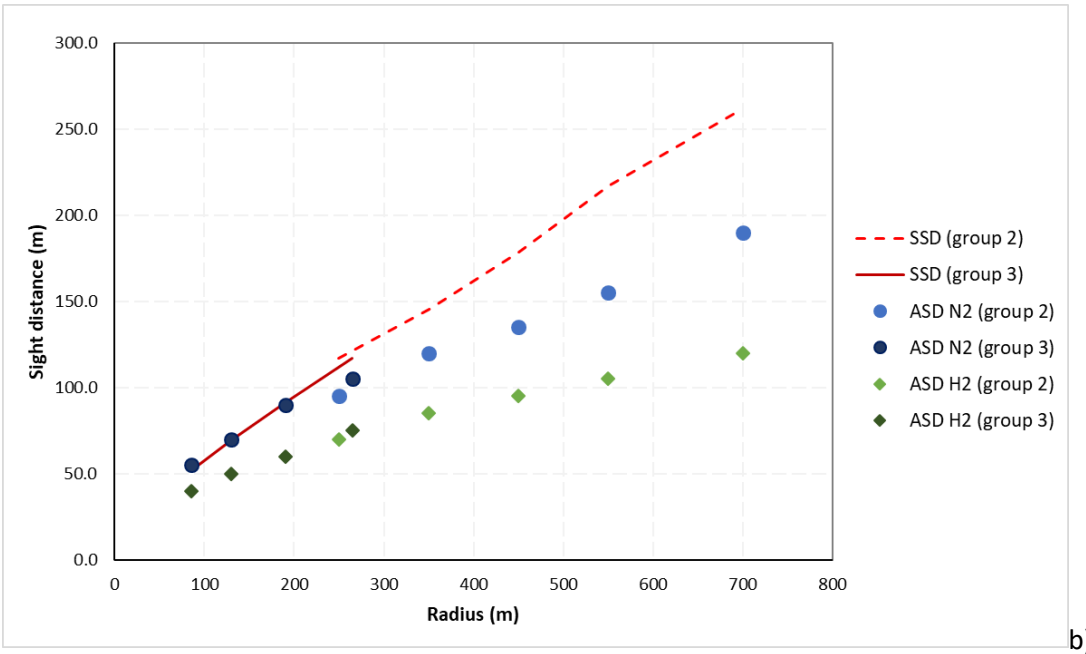

b)

Figure 7. Sight distance analysis as a function of the radius on horizontal curves overlapped with flat grade: a) left-hand curves, b) right-hand curves.

Considering the N2 barrier in left-hand curves (Figure 8a), the *ASD* is greater than the required *SSD* in all group 3 curves for both types of vertical profiles (flat and sag). The greatest *ASD* values are reached in the non-flat profile, with sag vertical curves. For group 2 curves the *SSD* is always guaranteed in the flat-grade terrain. However, the vertical profile with crest curves does not allow the *ASD* to meet the required SSD in curves with a larger radius (e.g. *ASD* = 225 m vs. *SSD* = 261.5 m for *R* = 700 m).

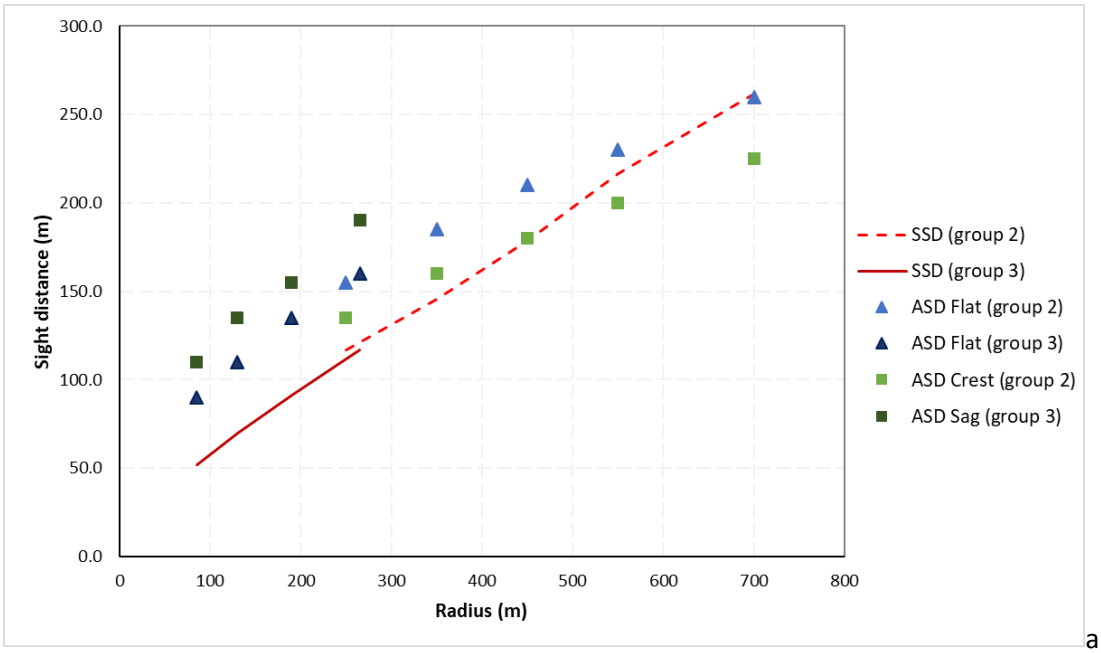

a)

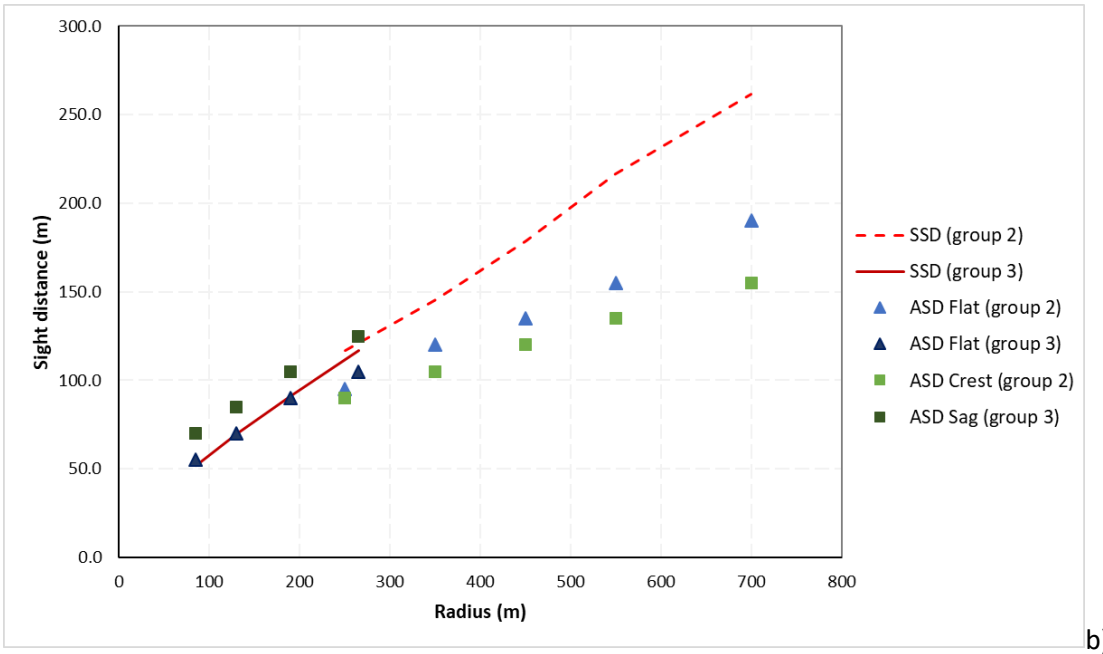

b)

Figure 8. Sight distance analysis in function of the radius on horizontal curves overlapped with N2 barrier: a) left-hand curves, b) right-hand curves.

Even considering two different vertical profiles, the situation in terms of *ASD* is critical for right-hand curves (Figure 8b). For group 3 curves, the sag vertical profile guarantees *ASD* > *SSD* in all curves; *ASD* values are lower than the required *SSD* for the group 2 curves, with both vertical profiles, especially with the flat-grade terrain.

By setting the H2 barrier in left-hand curves (Figure 9a), the *ASD* values exceeded the required *SSD* in all group 3 curves with both types of vertical profiles (flat and sag). In this case, sag vertical

curves provide better sight conditions as well. A different situation occurs for group 2 curves, where the *ASD* meets the required *SSD* just in the flat-grade terrain in the smallest curvature radii of the category (e.g. *ASD* = 125 m vs. *SSD* = 116.8 m for *R* = 250 m). This trend is again justified by the vertical profile: if the sag vertical curve provides a better sight distance, the crest one decreases the length of the road visible from the driver point of view.

In right-hand curves (Figure 9b), sight conditions do not comply with safety requirements in the presence of H2 guardrail, and the difference between *ASD* and *SSD* increases as the curve radius increases. *ASD* values for the flat-grade terrain and crest curve vertical profile are almost identical; in particular, in group 2, they coincide. This is attributable to the smaller distance between the driver and the sight obstruction (i.e., the guardrail), with the result that the same sight line is obtained for both cases (i.e., flat-grade and crest).

By analysing the *ASD* values for the two different vertical profiles, it can be observed that the presence of vertical curves impacts the sight distance: *ASD* increases in presence of sag curves (from *ASD*(N2) = 90 m and *ASD*(H2) = 75 m for "flat" profile to *ASD*(N2) = 110 m and *ASD*(H2) = 85 m for "sag" profile, for *R* = 85 m, left-hand curve; from *ASD*(N2) = 110 m and *ASD*(H2) = 90 m for "flat" profile to *ASD*(N2) = 135 m and *ASD*(H2) = 105 m for "sag" profile, for *R* = 130 m, left-hand-curve). Although safety conditions are usually met in the left-hand curves, it is clear that crest vertical curves decrease the *ASD* values (from *ASD*(N2) = 210 m and *ASD*(H2) = 170 m for "flat" profile to *ASD*(N2) = 180 m and *ASD*(H2) = 155 m for "crest" profile, for *R* = 450 m, left-hand curve).

The results documented in this manuscript are consistent with those obtained by Sarhan and Hassan (2012), where they found that crests provide reduced ASD values, while sags increase the ASD in comparison to the flat-grade terrain case in the presence of concrete barriers. In particular, as the absolute value of K_V decreases, *ASD* increases on sag curves and decreases on crests. Reduced lateral offsets were also found to affect negatively sight distance conditions. In this sense, the research results are also in line with preliminary results of the authors on existing highways in the presence of concrete barriers (De Santos-Berbel et al. 2018).

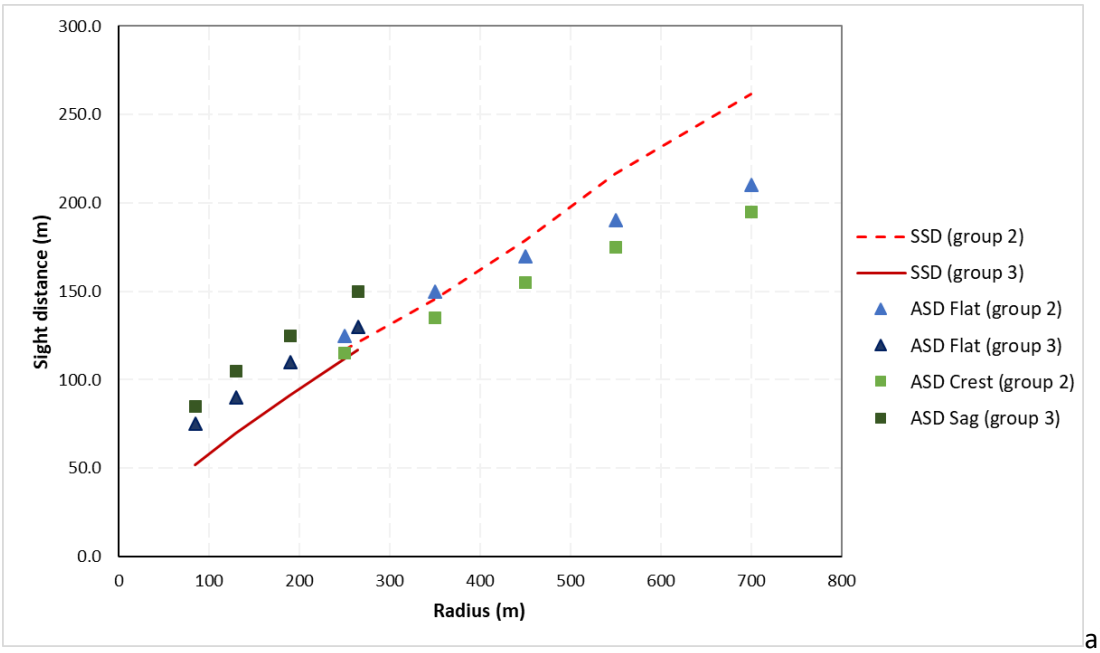

a)

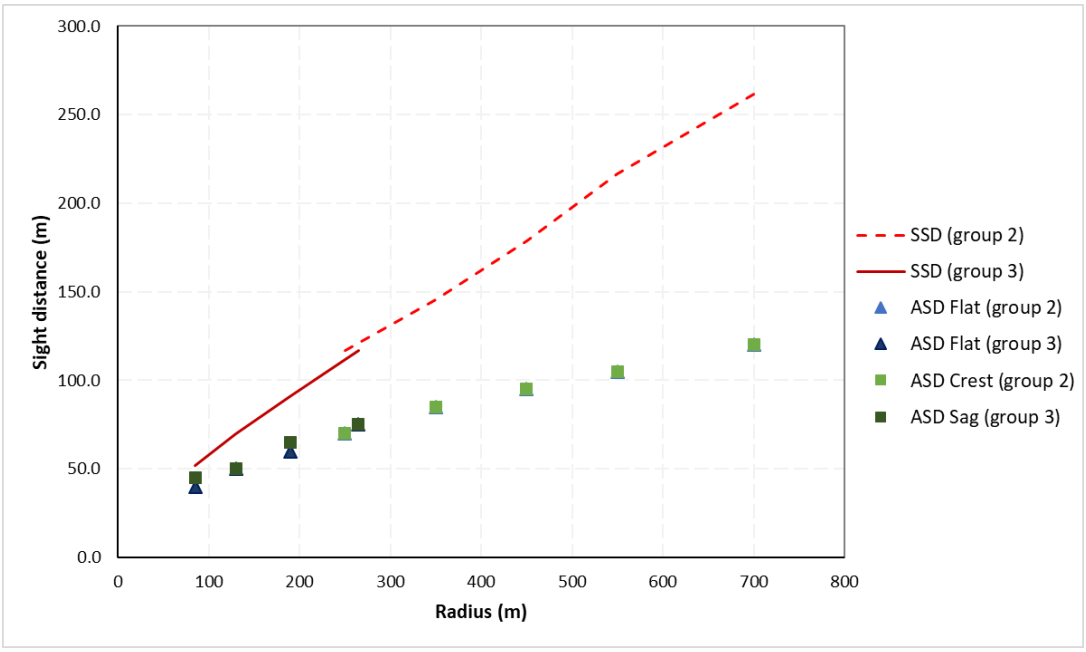

b)

Figure 9. Sight distance analysis as a function of the horizontal radius on curves overlapped with H2 barrier: a) left-hand curves, b) right-hand curves.

Conclusions

Research contribution

Previous studies demonstrated that GIS is a useful tool to carry out sight distance analyses on 3D models developed on existing road segments as well as on road projects. At present, no other modelling technique can provide reliable and fast results on road design scenarios. This study intended

to assess the variations of *ASD* due to different safety barrier types (i.e., their height) which can result from a difference in the design decision or cross-country difference in road standards. To this aim, the Shape Bender extension in the SketchUp Pro 2019 environment was used to adapt barriers to terrain models depicting different combinations of horizontal and vertical alignment. This tool greatly facilitates the 3D design, and it is particularly useful for roads and infrastructures.

GIS tools are useful to understand the effects of two different guardrail models on the *ASD* in curves. The use of multipatch features allows considering in the analysis sight obstruction previously modelled through 3D drawing software. As in this case, a faithful 3D reproduction of the guardrails allows to obtain reliable results, with a minimum of error, compared to other methods that may be more lacking.

Implications

Road designers should be aware of the impact of safety barriers on the *ASD* when considering the installation of barriers. The presence of taller barriers, even though they can provide greater containment levels, offer a reduced *ASD* value: in particular, worse visibility conditions detect in the presence of the 3-waves barrier (H2 guardrail) compared to the N2 type. Given that the N2 barrier has a lower height, it enabled greater *ASD*.

As the radius of the horizontal curve increases, it becomes more difficult to ensure *ASD* values that allow safe braking manoeuvres. It is demonstrated in group 2 curves (those with larger radii of curvature): as the radius increases, the difference between *SSD* and *ASD* increases too. This result is consistent with expectations because of the link between curve radii and design speed values (the higher the radius, the higher the design speed).

The worst sight conditions are certainly detected on right-hand curves. Comparing the curves, the *ASD* values are greater in the left-hand bends than in the right-hand ones. Again, this is consistent with expectations because of the dependence of *ASD* from the distance of the observer from the sight obstruction (the smaller the distance, the smaller the *ASD*).

From different comparisons involving the vertical profile and the dimensions of the curves, it is possible to see how the vertical profile affects the sight distance. Sag vertical curves increase *ASD* values, while the presence of horizontal curves overlapped with crest vertical curves worsens the sight conditions compared to a flat-grade terrain, especially in left-hand curves.

Limitations and future research needs

This work is limited to the specific road type and the two guardrails considered. Other analysis should be carried out with the aim of extend the results to different road and barrier typologies. Furthermore, the position for the barrier in the roadside (or in the median) is another factor that affects the *ASD* and that deserve specific analysis. The comparison between rigid and guardrails with different heights and shapes will provide other insight on the effects of these road furniture on the *ASD*.

As future lines of research, the authors are working on a driving simulator study to check whether the driver perceives and adapt their behavior to the different sight distance condition along curves treated with the two different barriers.

Data Availability Statement

Some or all data, models, or code that support the findings of this study are available from the corresponding author upon reasonable request.

Acknowledgments

The Spanish *Ministerio de Economía y Competitividad* and the European Regional Development Fund (FEDER) for research project TRA2015–63579-R (MINECO/FEDER), and the European Union Erasmus+ Programme funded this project. This Manuscript reflects the views only of the authors, and the Commission cannot be held responsible for any use which may be made of the information contained therein.

References

Alcón Gil, P., De Santos-Berbel, C., and Castro, M. (2021). "Driver glare exposure with different vehicle frontlighting systems." *Journal of Safety Research*, National Safety Council and Elsevier Ltd, 76, 228–237. https://doi.org/10.1016/j.jsr.2020.12.018

American Association of State Highway and Transportation Officials (AASHTO). (2011). *Roadside Design Guide*. Washington, D.C.

American Association of State Highway and Transportation Officials (AASHTO). (2018). *A policy on geometric design of highways and streets*. AASHTO, Washington, D.C.

Bassani, M., Grasso, N., and Piras, M. (2015). "3D GIS based evaluation of the available sight distance to assess safety of urban roads." *International Archives of the Photogrammetry, Remote Sensing and Spatial Information Sciences - ISPRS Archives*, 40, 137–143. https://doi.org/10.5194/isprsarchives-XL-3-W3-137-2015

Bassani, M., Grasso, N., Piras, M., and Catani, L. (2016). "Estimating the available sight distance on urban roads by integrating 3D maps and low-cost mobile mapping systems into a GIS numerical computing environment." *Transportation Research Board 95th Annual Meeting*, Washington D.C.

Bassani, M., Grasso, N., Piras, M., and Catani, L. (2019). "Estimating the available sight distance in the urban environment by GIS and numerical computing codes." *ISPRS International Journal of Geo-Information*, 8(2), 69. https://doi.org/10.3390/ijgi8020069

Campoy Ungria, J. M. (2015). "Nueva Metodología Para La Obtención De Distancias De Visibilidad Disponibles En Carreteras Existentes Basada En Datos Lidar Terrestre." Universidad Politécnica de Valencia, Valencia, Spain.

Castro, M., Anta, J. A., Iglesias, L., and Sánchez, J. A. (2014). "GIS-Based System for Sight Distance Analysis of Highways." *ASCE Journal of Computing in Civil Engineering*, 28(3): 04014005. https://doi.org/10.1061/(ASCE)CP.1943-5487.0000317

Castro, M., and De Santos-Berbel, C. (2015). "Spatial analysis of geometric design consistency and road

498 sight distance." *International Journal of Geographical Information Science*, 29(12), 2061–2074.
499 https://doi.org/10.1080/13658816.2015.1037304
500 Castro, M., De Santos-Berbel, C., and Iglesias, L. (2017). "A comprehensive methodology for the
501 analysis of highway sight distance." *Transport Infrastructure and Systems: Proceedings of the*
502 *AIIT*, 193–200, Rome, Italy: Associazione Italiana per l'Ingegneria del Traffico e dei Transporti.
503 Castro, M., Iglesias, L., Sánchez, J. Á., and Ambrosio, L. (2011). "Sight distance analysis of highways
504 using GIS tools." *Transportation Research Part C: Emerging Technologies*, 19(6), 997–1005.
505 https://doi.org/10.1016/j.trc.2011.05.012
506 Castro, M., López-Cuervo, S., Paréns-González, M., and de Santos-Berbel, C. (2016). "LIDAR-based
507 roadway and roadside modelling for sight distance studies." *Survey Review*, 48(350), 309–315.
508 https://doi.org/10.1179/1752270615Y.0000000037
509 De Santos-Berbel, C., Anta, J. A., Castro, M., and Iglesias, L. (2013). "Sight distance for road safety
510 analysis using GIS." *Esri Middle East Africa User Conference (EMEAUC)*, 1–9. Munich, Germany:
511 Esri Deutschland GmbH.
512 De Santos-Berbel, C., and Castro, M. (2018). "Three-dimensional virtual highway model for sight-
513 distance evaluation of highway underpasses." *Journal of Surveying Engineering*, 144(4),
514 05018003. https://doi.org/10.1061/(ASCE)SU.1943-5428.0000258
515 De Santos-Berbel, C., González-Gómez, K., Castro, M., and Anta, J. A. (2018). "Addressing sight-
516 distance-related safety effects of installing median barriers at horizontal curves of undivided
517 highways under a 3D approach." *5th International Conference on Road and Rail Infrastructure*
518 *(CETRA)*, 1067–1073. Zadar, Croatia: University of Zagreb.
519 Environmental Science Research Insitute (ESRI). (2008). *The multipatch geometry type*. Redlands,
520 California.
521 Environmental Science Research Institute (ESRI). (2021a). "Line of sight." Accessed May 28, 2021.
522 https://desktop.arcgis.com/en/arcmap/latest/tools/3d-analyst-toolbox/line-of-sight.htm
523 Environmental Science Research Institute (ESRI). (2021b). "Construct sight lines." Accessed May 28,

524 2021. https://desktop.arcgis.com/en/arcmap/latest/tools/3d-analyst-toolbox/construct-sight-
525 lines.htm
526 European Committee for Standardization (CEN). (2002). "ENV 1317-4. Road restraint systems. Part 4.
527 Performance classes, impact test acceptance criteria and test methods for terminals and
528 transitions of safety barriers."
529 European Committee for Standardization (CEN). (2011a). "EN 1317-1. Road restraint systems. Part 1:
530 Terminology and general criteria for test methods." Brussels, Belgium.
531 European Committee for Standardization (CEN). (2011b). "EN 1317-2. Road restraint systems. Part 2:
532 Performance classes, impact test acceptance criteria and test methods for safety barriers
533 including vehicle parapets."
534 European Committee for Standardization (CEN). (2012). "EN 1317-5. Road restraint systems. Part 5:
535 Product requirements and evaluation of conformity for vehicle restraint systems."
536 Gargoum, S. A., and El-Basyouny, K. (2020). "Analyzing the ability of crash-prone highways to handle
537 stochastically modelled driver demand for stopping sight distance." *Accident Analysis and*
538 *Prevention*, Elsevier, 136. https://doi.org/10.1016/j.aap.2019.105395
539 Gargoum, S. A., El-Basyouny, K., and Sabbagh, J. (2018). "Assessing Stopping and Passing Sight Distance
540 on Highways Using Mobile LiDAR Data." *Journal of Computing in Civil Engineering*, 32(4), 1–13.
541 https://doi.org/10.1061/(ASCE)CP.1943-5487.0000753
542 Ibrahim, S. E. B., and Sayed, T. (2011). "Developing safety performance functions incorporating
543 reliability-based risk measures." *Accident Analysis & Prevention*, Elsevier Ltd, 43(6), 2153–2159.
544 https://doi.org/10.1016/j.aap.2011.06.006
545 Iglesias, L., Castro, M., Pascual Gallego, V., and De Santos-Berbel, C. (2016). "Estimation of sight
546 distance on highways with overhanging elements." *3rd International Conference on Traffic and*
547 *Transport Engineering (ICTTE)*, 75–82. Belgrade, Serbia: City Net Scientific Research Center Ltd.
548 Iglesias, L., De Santos-Berbel, C., Pascual, V., and Castro, M. (2019). "Using small unmanned aerial
549 vehicle in 3D modeling of highways with tree-covered roadsides to estimate sight distance."

Remote Sensing, 11(2625), 1–13. https://doi.org/10.3390/rs11222625

Ismail, K. A., and Sayed, T. (2007). "New algorithm for calculating 3D available sight distance." *Journal of Transportation Engineering*, 133(10), 572–581. https://doi.org/10.1061/(ASCE)0733-947X(2007)133:10(572)

Jung, J., Olsen, M. J., Hurwitz, D. S., Kashani, A. G., and Buker, K. (2018). "3D virtual intersection sight distance analysis using lidar data." *Transportation Research Part C: Emerging Technologies*, Elsevier, 86(August 2017), 563–579. https://doi.org/10.1016/j.trc.2017.12.004

Khattak, A. J., and Shamayleh, H. (2005). "Highway safety assessment through geographic information system-based data visualization." *Journal of Computing in Civil Engineering*, 19(4), 407–411. https://doi.org/10.1061/(ASCE)0887-3801(2005)19:4(407)

Liu, C. (2013). "Exact sight distance determination on compound vertical and horizontal curves in the presence of road barriers." *International Journal of Transportation Science and Technology*, 2(2), 159–166. https://doi.org/10.1260/2046-0430.2.2.159

Ma, Y., Zheng, Y., Cheng, J., and Easa, S. M. (2019). "Real-time visualization method for estimating 3D highway sight distance using LiDAR data." *Journal of Transportation Engineering Part A: Systems*, 145(4): 04019006. https://doi.org/10.1061/JTEPBS.0000228

Ma, Y., Zheng, Y., Cheng, J., Guo, L., and Zhang, Y. (2018). "A novel real-time visualization algorithm for computing three- dimensional sight distance." *Transportation Research Board Annual Meeting*, (979).

Ministerio de Fomento. (2009). *Orden circular 28/2009 sobre criterios de aplicación de barreras de seguridad metálicas*. España.

Ministerio de Fomento. (2014). *Orden Circular 35/2014 sobre criterios de aplicación de sistemas de contención de vehículos*. España.

Ministerio de Fomento. (2016). *Instrucción de carreteras. Norma 3.1-IC*. España.

Ministero delle Infrastrutture e dei Trasporti. (2001). *Norme funzionali e geometriche per la costruzione delle strade*. Rome, Italy.

576 Ministero delle Infrastrutture e dei Trasporti. (2004). *Istruzioni tecniche per la progettazione,*
577 *l'omologazione e l'impiego dei dispositivi di ritenuta nelle costruzioni stradali*. Rome, Italy.
578 Montella, A. (2001). "Selection of roadside safety barrier containment level according to European
579 Union Standards." *Transportation Research Record*, (1743), 104–110.
580 https://doi.org/10.3141/1743-14
581 Papadimitriou, E., Mavromatis, S., and Psarianos, B. (2018). "Stopping sight distance adequacy
582 assessment on freeways: the case of left horizontal curves over crest vertical curves."
583 *Transportation Letters*, 10(5), 269–279. https://doi.org/10.1080/19427867.2016.1259759
584 Sarhan, M., and Hassan, Y. (2012). "Consideration of sight distance in placement of concrete barriers
585 on horizontal curves of roads." *Transportation Research Record*, (2301), 9–16.
586 https://doi.org/10.3141/2301-02
587 Shalkamy, A., El-Basyouny, K., and Xu, H. Y. (2020). "Voxel-based methodology for automated 3d sight
588 distance assessment on highways using mobile light detection and ranging data." *Transportation*
589 *Research Record*, 2674(5), 587–599. https://doi.org/10.1177/0361198120917376
590 Steinauer, B., and Mayer, G. (1999). "Sicherheitsdefizite in der Straßenplanung." *Straße und Autobahn*,
591 12(99), 655–662.
592 TOOL S.A. (2013). *Manual de instrucciones del programa CLIP sobre windows*. Madrid, Spain. TOOL,
593 S.A.
594 Trimble. (2013). "Extension Warehouse: CLF Shape Bender tool." Accessed December 6, 2020.
595 https://extensions.sketchup.com/extension/8a4d10ff-40f3-4885-b8ba-1dac2b941885/clf-
596 shape-bender
597 Wang, J., Lawson, G., and Shen, Y. (2014). "Advances in Engineering Software Automatic high-fidelity
598 3D road network modeling based on 2D GIS data." *Advances in Engineering Software*, Elsevier
599 Ltd, 76, 86–98. https://doi.org/10.1016 716/j.advengsoft.2014.06.005
600 Wang, J., Zhou, H., and Zhang, Y. (2017). "Improve sight distance at signalized ramp terminals of
601 partial-cloverleaf interchanges to deter wrong-way entries." *Journal of Transportation*

602 *Engineering*, 143(6), 04017017. https://doi.org/10.1061/JTEPBS.0000039